ADVANCED ENERGY MATERIALS
www.advenergymat.de

# The Impact of Device Polarity on the Performance of Polymer–Fullerene Solar Cells

*Mengmeng Li, Junyu Li, Dario Di Carlo Rasi, Fallon J. M. Colberts, Junke Wang, Gaël H. L. Heintges, Baojun Lin, Weiwei Li, Wei Ma, Martijn M. Wienk, and René A. J. Janssen**

**Diketopyrrolopyrrole (DPP)-conjugated polymers are a versatile class of semiconductors for application in organic solar cells because of their tunable optoelectronic properties. A record power conversion efficiency (PCE) of 9.4% was recently achieved for DPP polymers, but further improvements are required to reach true efficiency limits. Using five DPP polymers with different chemical structures and molecular weights, the device performance of polymer:fullerene solar cells is systematically optimized by considering device polarity, morphology, and light absorption. The polymer solubility is found to have a significant effect on the optimal device polarity. Soluble polymers show a 10–25% increase in PCE in inverted device configurations, while the device performance is independent of device polarity for less soluble DPP derivatives. The difference seems related to the polymer to fullerene weight ratio at the ZnO interface in inverted devices, which is higher for more soluble DPP polymers. Optimization of the nature of the cosolvent to narrow the fibril width of polymers in the blends toward the exciton diffusion length enhances charge generation. Additionally, the use of a retroreflective foil increases absorption of light. Combined, the effects afford a PCE of 9.6%, among the highest for DPP-based polymer solar cells.**

## 1. Introduction

In recent years, bulk heterojunction (BHJ) polymer:fullerene solar cells have attracted much attention due to their potential in solution-processable, low-cost, large-scale, light-weight, and flexible plastic electronics as renewable energy sources.[1–3] Diketopyrrolopyrrole (DPP)-based polymers are a versatile class of organic semiconducting materials, used extensively in polymer:fullerene solar cells.[4] As donor–acceptor conjugated polymers, rational design and synthesis can be used to tune the optical bandgap and frontier orbital energy levels to optimize absorption of light and the photon-to-charge conversion efficiency.[4] For instance, by modifying the aromatic substituents and $\pi$–conjugated segments, the optical properties of DPP-based polymers can be manipulated from small (1.13 eV) to wide bandgaps (1.77 eV).[5–7] In particular, DPP-based polymers bridged with thiazole units exhibited external quantum efficiencies (EQEs) over 50% with an energy loss between optical bandgap and open-circuit voltage below 0.6 eV in polymer:fullerene solar cells.[8]

The impact of device polarity on the photovoltaic performance is still under debate, although the inverted (n–i–p) device structure has become more popular than the conventional (p–i–n) configuration.[9,10] It has been proposed that the use of acidic poly(ethylenedioxythiophene):poly(styrene sulfonate) (PEDOT:PSS) and reactive metals such as Al in the conventional device configuration cause issues regarding the device stability and performance,[1] and that inverted devices are capable of enhancing the optical electric field and improving the interfacial contact.[7,11] Several examples of DPP-based polymers revealed the advantageous effects of inverted structure with superior power conversion efficiency (PCE) over 8%.[11–14] However, the record efficiency of solar

Dr. M. Li, D. Di Carlo Rasi, F. J. M. Colberts, J. Wang, G. H. L. Heintges, Dr. M. M. Wienk, Prof. R. A. J. Janssen
Molecular Materials and Nanosystems
Institute for Complex Molecular Systems
Eindhoven University of Technology
P.O. Box 513, Eindhoven MB 5600, The Netherlands
E-mail: r.a.j.janssen@tue.nl

The ORCID identification number(s) for the author(s) of this article can be found under https://doi.org/10.1002/aenm.201800550.

© 2018 The Authors. Published by WILEY-VCH Verlag GmbH & Co. KGaA, Weinheim. This is an open access article under the terms of the Creative Commons Attribution-NonCommercial License, which permits use, distribution and reproduction in any medium, provided the original work is properly cited and is not used for commercial purposes.

DOI: 10.1002/aenm.201800550

Dr. J. Li
DSM DMSC R&D Solutions
P.O. Box 18, Geleen MD 6160, The Netherlands

B. Lin, Prof. W. Ma
State Key Laboratory for Mechanical Behavior of Materials
Xi'an Jiaotong University
Xi'an 710049, P. R. China

Prof. W. Li
Beijing National Laboratory for Molecular Sciences
CAS Key Laboratory of Organic Solids
Institute of Chemistry
Chinese Academy of Sciences
Beijing 100190, P. R. China

Dr. M. M. Wienk, Prof. R. A. J. Janssen
Dutch Institute for Fundamental Energy Research
De Zaale 20, Eindhoven AJ 5612, The Netherlands

 © 2018 The Authors. Published by WILEY-VCH Verlag GmbH & Co. KGaA, Weinheim

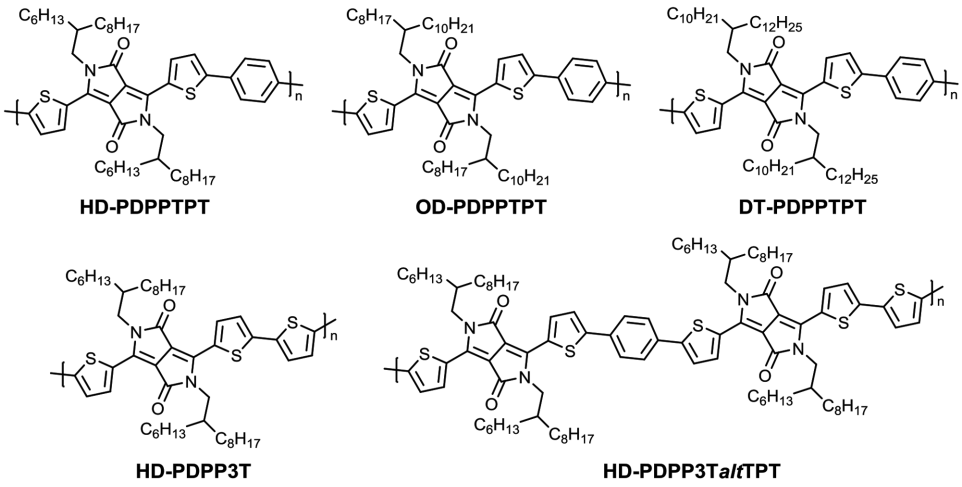


**Figure 1.** Chemical structures of diketopyrrolopyrrole (DPP)-based polymers used in this study.

cells based on DPP polymers so far was achieved using a conventional polarity device, exhibiting PCEs of >9%.[15,16] Unfortunately, a one-to-one comparison for high-efficiency polymer solar cells has been rarely reported, which blurs our understanding of the intrinsic role of the device polarity on the PCE.

In this contribution, we evaluated five DPP-based polymers with various chemical structures, including alkyl chains on the DPP units and backbones, and molecular weights (**Figure 1**), and demonstrate that the polymer solubility has a crucial role on the optimal device polarity. For polymers with good solubility, inverted devices showed a 10–25% improvement in photovoltaic performance compared to conventional one. In contrast, identical PCEs were observed for less soluble polymers, independent of device polarity. To further boost the performance of polymer solar cells, the cosolvent for solution processing was carefully optimized to narrow the width of the semicrystalline fibrils of the DPP polymers to the exciton diffusion length, resulting in an enhanced charge generation. Additionally, a retroreflective foil was utilized to capture more light for solar cells. When combined the optimization resulted in a PCE of 9.6%, which is a new record for solar cells based on DPP polymers. More importantly, we provide general and systematic procedures to optimize the device performance of solution-processed polymer solar cells.

## 2. Results and Discussion

### 2.1. Conventional or Inverted Polarity?

#### *2.1.1. Effect of Polymer Structure*

To verify the influence of device polarity on the performance of polymer solar cells, all processing parameters including polymer:[6,6]-phenyl-$C_{71}$-butyric acid methyl ester ([70]PCBM) ratio, polymer concentration, and solvent/cosolvent were kept constant, while the thickness of the active layer was optimized (vide infra). First, a blend of poly[{2,5-bis(2-hexyldecyl)-2,3,5,6-tetrahydro-3,6-dioxopyrrolo[3,4-c]pyrrole-1,4-diyl}-*alt*-{[2,2′-(1,4-phenylene)bisthiophene]-5,5′-diyl}] (**HD-PDPPTPT**:) with [70]PCBM (1:2 w/w) was investigated in a conventional device configuration using a transparent indium tin oxide (ITO)/PEDOT:PSS front contact and a reflective LiF/Al back contact (**Figure 2**a). The optimized thickness of the photoactive layer was 110 nm. The short-circuit current densities ($J_{sc,sr}$) for determining the PCEs were obtained by integrating the EQEs spectrum with AM1.5G spectrum. This is a more accurate way of determining the short-circuit current density. The resultant conventional-polarity cell exhibited a good photovoltaic behavior with a PCE of 7.4%, in agreement with our previous report.[17] Next, an inverted device (ITO/ZnO/**HD-PDPPTPT**:[70]PCBM/$MoO_x$/Ag) was fabricated with an optimized film thickness of 90 nm. The inverted polarity device results in a ≈13% improvement in photocurrent ($J_{sc,sr}$) from 14.0 to 15.8 mA cm$^{-2}$, while both open-circuit voltage ($V_{oc}$) and fill factor (FF) remained unchanged, leading to an increased PCE of 8.4% (Figure 2b). Figure 2c shows the spectrally resolved EQEs. An enhanced EQE for the inverted device can be seen in the regions of 450–580 and 650–800 nm, corresponding to the optical absorption range of [70]PCBM and **HD-PDPPTPT**, respectively.[18]

To rationalize the origin of photocurrent improvement by changing the device polarity, the different aspects were considered. First, the inverted device employs sol–gel ZnO as an electron transport layer. This creates a unique rough surface, featuring a self-organized ripple nanostructure[19] with a root-mean-square roughness ($R_q$) of around 3.3 nm (Figure S1 in the Supporting Information). The morphology of blend films for both conventional and inverted cells was determined from transmission electron microscopy (TEM, Figure S2, Supporting Information). Identical fibrillar nanostructures with a fibril width of around 7 nm indicate negligible effect of the rough ZnO layer on the self-assembly in the bulk of the **HD-PDPPTPT**:[70]PCBM blend. It has been proposed that ZnO nanoripples are capable of inducing scattering to enhance the light absorption in the active layer in organic photovoltaics (OPV).[20] In the absence of electrodes, we found however that the effect of the nanoripples on the film absorption is negligible, and that the film thickness primarily determines light absorption (Figure S3, Supporting Information).

Theoretical analysis by optical modeling was also used to compare light absorption in conventional and inverted polarity


© 2018 The Authors. Published by WILEY-VCH Verlag GmbH & Co. KGaA, Weinheim

16146840, 2018, 22, Downloaded from https://onlinelibrary.wiley.com/doi/10.1002/aenm.201800550 by Univ of California Lawrence Berkeley National Lab, Wiley Online Library on [22/02/2024]. See the Terms and Conditions (https://onlinelibrary.wiley.com/terms-and-conditions) on Wiley Online Library for rules of use; OA articles are governed by the applicable Creative Commons License

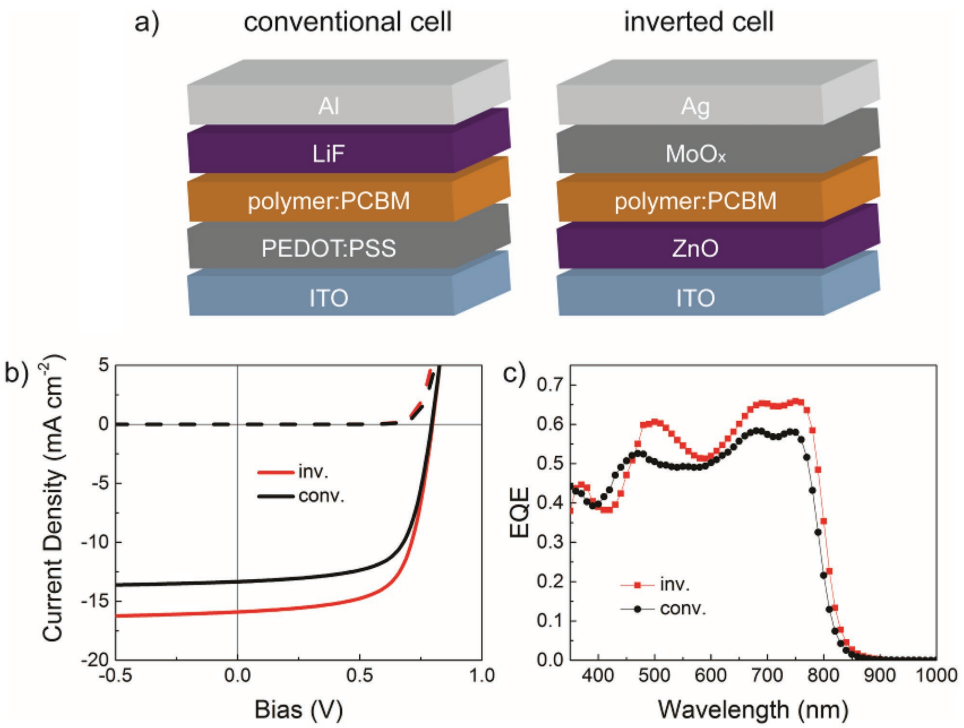


**Figure 2.** a) Device configurations of polymer solar cells with conventional (p–i–n) and inverted (n–i–p) polarity. b) *J–V* characteristics and c) spectrally resolved EQE of **HD-PDPPTPT**:[70]PCBM (1:2 w/w) solar cells.

devices. In the presence of electrodes, the optically modeled absorption spectra demonstrate that, compared to a conventional device layout, the inverted polarity configuration results in a small red-shift of the peak at ≈480 nm (mainly due to [70]PCBM) and an enhanced absorption in the 650–800 nm region where the polymer absorbs (Figure S4, Supporting Information), consistent with measured EQEs (Figure 2c). Photocurrents as a function of thickness of blend film were theoretically estimated (Figure S5, Supporting Information). Although optical modeling confirms the function of $MoO_x$ as an optical spacer by shifting the position of the maximum optical field into the active layer and reproduces the optimized thicknesses of 110 and 90 nm,[21] the difference in the maximum calculated $J_{sc}$ between conventional and inverted devices is only 0.3 mA cm$^{-2}$. This is much lower than the experimental result ($\Delta J_{sc}$ = 1.8 mA cm$^{-2}$).

We therefore conclude that the superior performance of the inverted polarity for **HD-PDPPTPT**:[70]PCBM (1:2 w/w) devices cannot be attributed to bulk film morphology or enhanced optical absorption and must have a different origin.

Similar effects of device polarity on photovoltaic performance were observed for other two DPP-based polymers. Compared to **HD-PDPPTPT**, poly[{2,5-bis(2-decyltetradecyl)-2,3,5,6-tetrahydro-3,6-dioxopyrrolo[3,4-*c*]pyrrole-1,4-diyl}-*alt*-{[2,2′-(1,4-phenylene)bisthiophene]-5,5′-diyl}] (**DT-DT-PDPPTPT**), and poly[{2,5-bis(2-octyldodecyl)-2,3,5,6-tetrahydro-3,6-dioxopyrrolo[3,4-*c*]pyrrole-1,4-diyl}-*alt*-{[2,2′-(1,4-phenylene)bisthiophene]-5,5′-diyl}] (**OD-PDPPTPT**) possess longer alkyl chains on the DPP units, increasing polymer solubility. For inverted devices the $V_{oc}$ was slightly reduced by 0.01–0.02 V, but the FF was improved to over 0.70. Additionally, a significant enhanced photocurrent, by 0.7–1.1 mA cm$^{-2}$, was achieved, improving the cell efficiency from 5.2% to 6.1% for **OD-PDPPTPT** and from 4.4% to 4.9% for **DT-PDPPTPT** (Table 2; Figure S6, Supporting Information). Compared to **HD-PDPPTPT**, the improvement of EQE only occurred in the absorption range of the polymer (650–800 nm) in both cases, as shown in **Figure 3**.

Our previous work revealed that the polymer solubility critically affects the device performance of polymer solar cells.[22] In particular, we have demonstrated that less soluble DPP polymers result in thinner semicrystalline polymer fibers, governed by a nucleation-and-growth mechanism.[22] These thinner fibers for less-soluble DPP polymers enhance photoinduced charge generation, because a larger fraction of excitons can diffuse to the donor–acceptor interface where they generate electrons and holes.[17] All three **PDPPTPT** polymers (with HD, OD, and DT side chains) investigated in this study have good solubility in chloroform, so an interesting question arises: is the advantageous effect of the inverted polarity dependent on the polymer solubility? To answer this question, two other polymers with limited solubility, poly[[2,5-bis(2-hexyldecyl)-2,3,5,6-tetrahydro-3,6-dioxopyrrolo[3,4-c]pyrrole-1,4-diyl][2,2′:5′,2″-terthiophene]-5,5″-diyl[2,5-bis(2-hexyldecyl)-2,3,5,6-tetrahydro-3,6-dioxopyrrolo[3,4-c]pyrrole-1,4-diyl]-2,5-thiophene-1,4-phenylene-2,5-thiophenediyl] (**HD-PDPP3T*alt*TPT**) and poly[[2,5-bis(2-hexyldecyl)-2,3,5,6-tetrahydro-3,6-dioxopyrrolo[3,4-c]pyrrole-1,4-diyl]-*alt*-[2,2′:5′,2″-terthiophene]-5,5″-diyl] (**HD-PDPP3T**), were evaluated in solar cells. A high temperature of 90 °C was required to dissolve **HD-PDPP3T** and **HD-PDPP3T*alt*TPT** in superheated chloroform, and the solution had to be used within 20 min after preparation, because the limited solubility led to the formation of gel in 2 h (see insets in Figures 3 and 5a). In


© 2018 The Authors. Published by WILEY-VCH Verlag GmbH & Co. KGaA, Weinheim

16146840, 2018, 22, Downloaded from https://onlinelibrary.wiley.com/doi/10.1002/aenm.201800550 by Univ of California Lawrence Berkeley National Lab, Wiley Online Library on [22/02/2024]. See the Terms and Conditions (https://onlinelibrary.wiley.com/terms-and-conditions) on Wiley Online Library for rules of use; OA articles are governed by the applicable Creative Commons License

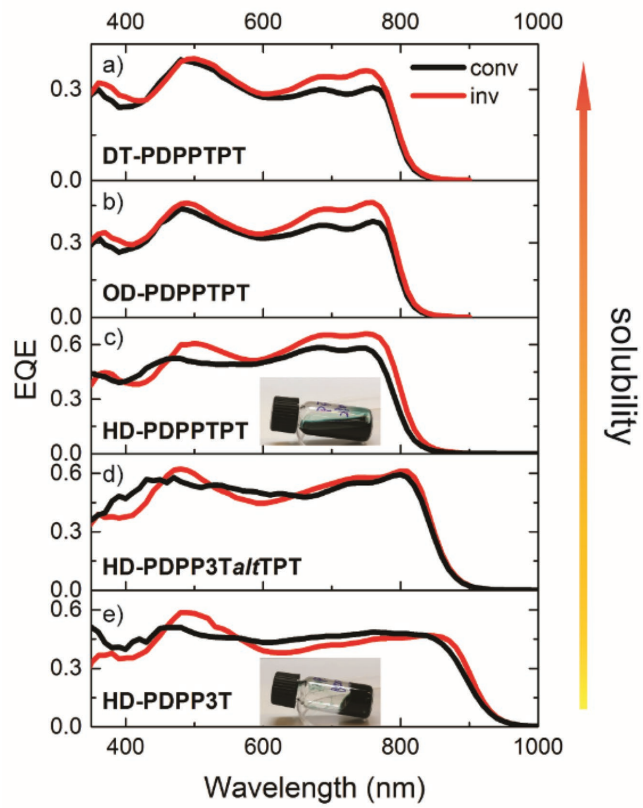


**Figure 3.** EQE of a) **DT-PDPPTPT**:[70]PCBM, b) **OD-PDPPTPT**:[70]PCBM, c) **HD-PDPPTPT**:[70]PCBM, d) **HD-PDPP3T*alt*TPT**:[70]PCBM, and e) **HD-PDPP3T**: [70]PCBM with conventional (conv.) and inverted (inv.) polarities. For each layer the polymer:fullerene weight ratio was 1:2. Chloroform was used as the main solvent for processing in all cases. From bottom to top, the solubility of polymer is increasing. The weight average molecular weight ($M_w$) of **HD-PDPP3T** is 400 kg mol$^{-1}$. The image in the bottom panel shows gel formation within 2 h due to the limited solubility, while the more soluble polymer (middle panel) remains well dissolved.

remarkable contrast to the three more soluble **PDPPTPT** polymers, the photovoltaic performance of the less soluble **HD-PDPP3T*alt*TPT** and **HD-PDPP3T** polymers was independent of device polarity. For **HD-PDPP3T** ($M_w$ = 400 kg mol$^{-1}$), the EQE of the inverted device was clearly reduced in the 600–800 nm region, which was compensated by an enhanced [70]PCBM contribution at 450–550 nm, as shown in Figure 3e. Therefore, similar photocurrents were obtained, leading to a polarity-independent performance. The same trend was observed for **HD-PDPP3T*alt*TPT** (Figure 3).

As a result, the systematical investigation of five DPP-based polymers with various side chains and backbones demonstrates that the inverted device exhibits better performance than the conventional one for more soluble polymers, while identical performance is achieved for less soluble polymers. Note that these DPP-based polymers generally show very similar charge carrier mobilities with values on the order of $10^{-2}$ cm$^2$ V$^{-1}$ s$^{-1}$,[18,23] and therefore the effect of mobility on the resultant PCE is negligible in this study.

### 2.1.2. Effect of Molecular Weight

To obtain more insight into the effect of the polymer solubility on the preferred device configuration, three other batches of **HD-PDPP3T** with lower molecular weights ($M_w$ = 79, 157, and 255 kg mol$^{-1}$) were synthesized (Scheme S1 and Table S1, Supporting Information), and their photovoltaic properties were studied in BHJ solar cells. In this way, the impact of chemical structure on the morphology and subsequent device performance is reduced, and the intrinsic role of solubility can be better clarified. The decrease in $M_w$ efficiently improved the polymer solubility (insets in Figure 5a). In particular, a temperature of 60 °C was sufficient to dissolve polymers with $M_w$ = 79 and 157 kg mol$^{-1}$ in chloroform. TEM was performed to determine the morphology of **HD-PDPP3T**:[70]PCBM blend (1:2 w/w) films. Similar fibrillar microstructures are observed, but as a result of the improved solubility the fibrils become wider from 12.9 nm for $M_w$ = 400 kg mol$^{-1}$ to 16.5 nm for $M_w$ = 79 kg mol$^{-1}$, as shown in **Figure 4**a,b. Besides, the out-of-plane profiles of grazing incident wide angle X-ray scattering (GIWAXS, Figure 4c; Figure S7, Supporting Information) present a sharper shoulder peak at $q$ = 1.72 Å$^{-1}$ (corresponding to a $\pi$–$\pi$ stacking distance of 3.65 Å) for $M_w$ = 400 kg mol$^{-1}$ compared to $M_w$ = 70 kg mol$^{-1}$. The corresponding coherence length ($L_{CH}$) was calculated by using the full width at half maximum (FWHM) of this reflection peak. The value of $L_{CH}$ is 2.2 nm for $M_w$ = 400 kg mol$^{-1}$, almost doubled compared to $L_{CH}$ = 1.2 nm for $M_w$ = 70 kg mol$^{-1}$. A longer $L_{CH}$ evidences a more ordered structure, which facilitates charge separation and charge carrier transport.

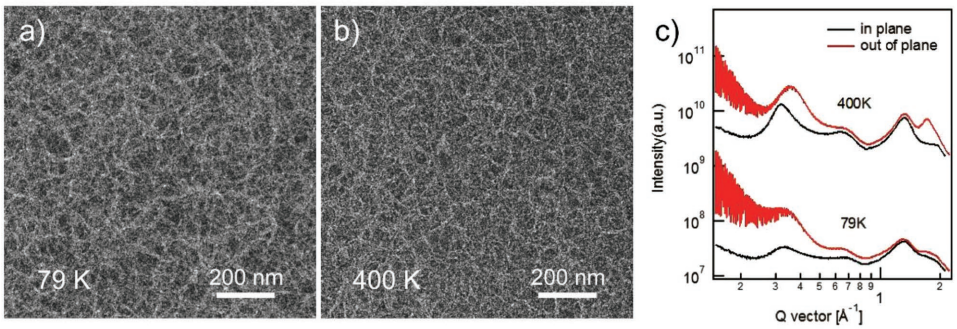


**Figure 4.** a,b) TEM images and c) GIWAXS in-plane and out-of-plane profiles of **HD-PDPP3T**:[70]PCBM blend films (1:2 w/w) with various $M_w$.


© 2018 The Authors. Published by WILEY-VCH Verlag GmbH & Co. KGaA, Weinheim

16146840, 2018, 22, Downloaded from https://onlinelibrary.wiley.com/doi/10.1002/aenm.201800550 by Univ of California Lawrence Berkeley National Lab, Wiley Online Library on [22/02/2024]. See the Terms and Conditions (https://onlinelibrary.wiley.com/terms-and-conditions) on Wiley Online Library for rules of use; OA articles are governed by the applicable Creative Commons License

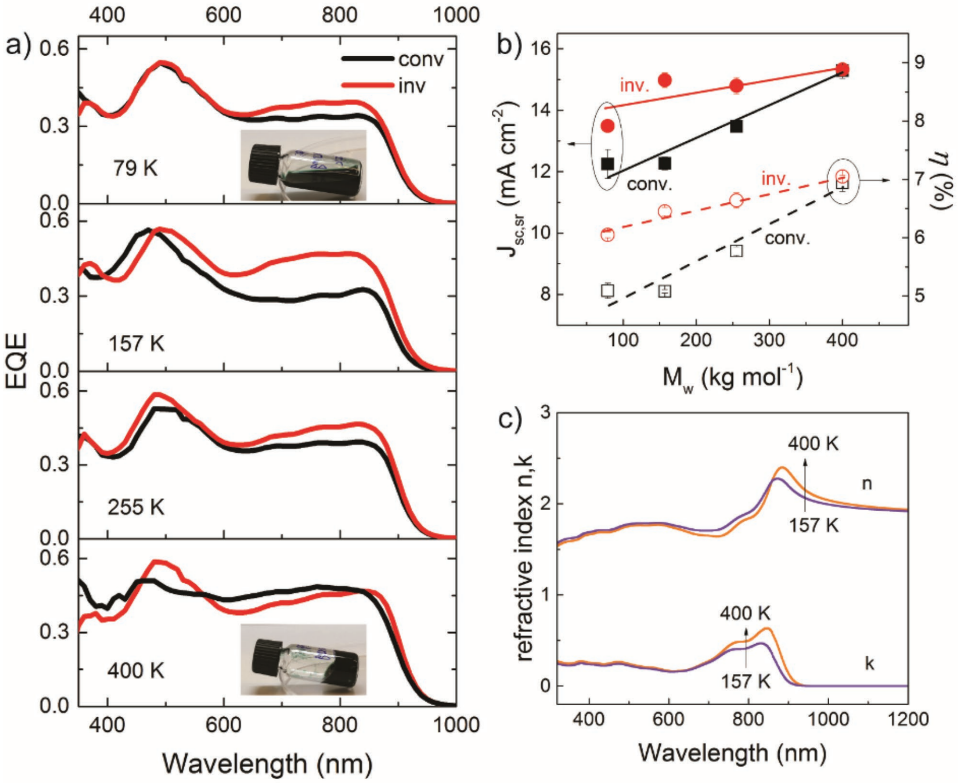


**Figure 5.** a) EQE spectra of **HD-PDPP3T**:[70]PCBM blend (1:2 w/w) films with various $M_w$. The bottom inset image shows gel formation in 2 h due to the limited solubility, while low-$M_w$ polymer (top inset) remains well dissolved in solution. b) The dependence of $J_{sc,sr}$ and PCE ($\eta$) on $M_w$. The solid and dashed lines are guides to the eye. c) Refractive index ($n$,$k$) data of **HD-PDPP3T**:[70]PCBM blend films.

For these three low-$M_w$ **HD-PDPP3T** samples, the inverted devices outperform the conventional ones without affecting $V_{oc}$ and FF (Figures S8 and S9, Supporting Information). The EQE spectra in **Figure 5**a manifest the enhanced photon-to-electron conversion efficiency in the polymer region by employing an inverted polarity, which is the main contributor to the performance improvement. Figure 5b summarizes $J_{sc,sr}$ and PCE ($\eta$) as a function of $M_w$. It is clear that the improvement in photovoltaic performance by using inverted polarity becomes more pronounced when the polymer solubility is increased by decreasing $M_w$.

Note that in both inverted and conventional devices the cell performance is improved by increasing $M_w$ which results in narrower fibrils (Figure 4). Recently, it was proposed that such $M_w$ dependent efficiency can be attributed to enhanced optical absorption for higher $M_w$ polymers.[13] To verify this possibility and its relation with the observed advantageous effect of inverted polarity, the refractive index ($n$) and extinction coefficient ($k$) of **HD-PDPP3T**:[70]PCBM blend films were measured. Because of their biggest and smallest efficiency difference between inverted and conventional devices, the polymers with $M_w$ = 157 kg mol$^{-1}$ and $M_w$ = 400 kg mol$^{-1}$ were selected for the measurements. The experiments confirm that the $k$ value at 840 nm is increased from 0.46 for $M_w$ = 157 kg mol$^{-1}$ to 0.63 for $M_w$ = 400 kg mol$^{-1}$ (Figure 5c), suggesting more efficient light absorption for higher $M_w$. This enhanced absorption could be attributed to higher persistence length of the polymer.[13]

The theoretical photocurrents obtained for **HD-PDPP3T**:[70]PCBM (1:2 w/w) with $M_w$ of 157 and 400 kg mol$^{-1}$ (Figure S10, Supporting Information) were calculated from $n$ and $k$ values using optical modeling (Figure 5c). The maximum value of the theoretical $J_{sc}$ for the $M_w$ = 400 kg mol$^{-1}$ batch is higher by ≈1.5 mA cm$^{-2}$ than for the $M_w$ = 157 kg mol$^{-1}$ material, both in conventional and inverted cells (**Table 1**). More importantly, the inverted devices are proven to always show better performance than the conventional ones with $\Delta J_{sc} \approx 0.7$ mA cm$^{-2}$ independent of $M_w$ (Table 1). In comparison, the experimental data exhibit a different trend. With lower $M_w$ such as 157 kg mol$^{-1}$, inverted devices exhibit 3.1 mA cm$^{-2}$ higher $J_{sc}$ than the conventional ones, and this difference is over fourfold larger than the simulated results (0.7 mA cm$^{-2}$, Table 1). On the contrary, higher $M_w$ of 400 kg mol$^{-1}$ performs almost independent of device polarity, although the theoretical simulation still shows stronger light absorption and higher photocurrent for the inverted device (Figure S10, Supporting Information). These results provide further evidence for the advantageous effect of inverted polarity for soluble polymers, as concluded in Section 2.1.1.

### 2.1.3. Hypothesis of Polarity Effect

It is useful to define the difference in PCE between conventional and inverted devices as $\Delta\eta = (\eta_{inv} - \eta_{conv})/\eta_{conv}$, where $\eta_{conv}$ and $\eta_{inv}$ are the PCEs for conventional and inverted polarity devices,


© 2018 The Authors. Published by WILEY-VCH Verlag GmbH & Co. KGaA, Weinheim

16146840, 2018, 22, Downloaded from https://onlinelibrary.wiley.com/doi/10.1002/aenm.201800550 by Univ of California Lawrence Berkeley National Lab, Wiley Online Library on [22/02/2024]. See the Terms and Conditions (https://onlinelibrary.wiley.com/terms-and-conditions) on Wiley Online Library for rules of use; OA articles are governed by the applicable Creative Commons License

**Table 1.** Comparison of $J_{sc,sr}$ between the simulation and measurement for **HD-PDPP3T**:[70]PCBM (1:2 w/w) as a function of $M_w$.

| | $M_w$ [kg mol$^{-1}$]/PDI (–) | $J_{sc,max}$ [mA cm$^{-2}$] | | $\Delta J_{sc,max}$ [mA cm$^{-2}$] |
|---|---|---|---|---|
| | | conv. | inv. | |
| simulation | 157/2.1 | 23.4 | 24.1 | 0.7 |
| | 400/2.7 | 24.8 | 25.6 | 0.8 |
| measurement | 157/2.1 | 12.0 | 15.1 | 3.1 |
| | 400/2.7 | 15.4 | 15.5 | 0.1 |

respectively. **Figure 6** plots the relation between the solubility and $\Delta\eta$. We manipulate the polymer solubility in two ways: 1) by modifying the chemical structures including the side chains and polymer backbones; 2) by varying the molecular weight. In both cases, we draw the same conclusion that the solar cells with inverted polarity exhibit better performance than the conventional device for polymers with good solubility, and higher PCE is achievable ($\Delta\eta$ = 10%–25%), which is mainly attributed to improvement of $J_{sc}$. In contrast, the cell performance is independent of device polarity for less soluble polymers, i.e. $\Delta\eta \approx 0$.

To further understand the origin of the improved performance caused by inverted configuration, X-ray photoelectron spectroscopy (XPS) depth profiles were recorded for **HD-PDPP3T**:[70]PCBM (1:2 w/w) layers processed on ZnO (inverted structure) (**Figure 7**). Both surface and bulk of the photoactive layer show a constant atom concentration for C, S, and N. Therefore, more attention is paid to the interface between photoactive layer and ZnO. For $M_w$ = 157 kg mol$^{-1}$ ($\eta_{inv} > \eta_{conv}$), the C atom concentration starts to drop at 1900 s, while the concentrations for N and S (exclusively from the polymer) remain constant until 2140 s (Figure 7a). This indicates that the ratio of polymer to [70]PCBM is increased close to the ZnO interface. On the contrary, the reduction in atom concentration of N and S follows the trend of C for $M_w$ = 400 kg mol$^{-1}$ ($\eta_{inv} \approx \eta_{conv}$) (Figure 7b). A clearer difference induced by polymer solubility is shown using N/C and S/C atom ratios (Figure 7c,d). Low $M_w$ results in a noticeable enhancement of the N/C and S/C atom ratios starting at 2035 s, suggesting an increased amount polymer (decreased [70]PCBM) at the ZnO interface. On the other hand, both N/C and S/C remain almost unchanged for the high $M_w$ material, even at the ZnO interface. The corresponding conventional devices were also analyzed by XPS; however, the quantitative analysis of atom ratio between polymer to [70]PCBM is impractical because PEDOT:PSS contains both C and S. Further evidence is provided by measuring inverted device for **HD-PDPPTPT**:[70]PCBM ($\eta_{inv} > \eta_{conv}$). Similar behavior to low-$M_w$ **HD-PDPP3T** is observed with the increase in N/C and S/C ratios at ZnO interface (Figure S11, Supporting Information).

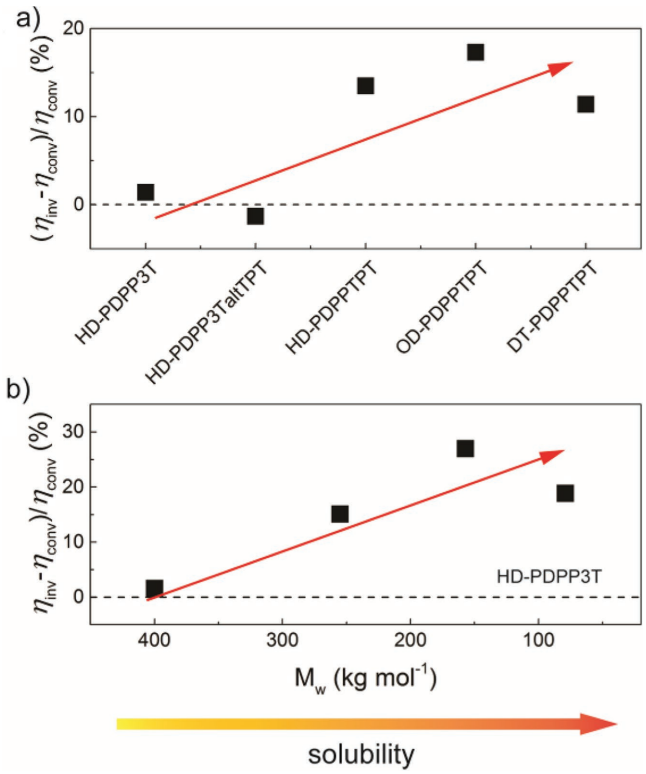


**Figure 6.** The influence of polymer solubility on the performance difference between conventional and inverted devices. a) Solubility in chloroform: **HD-PDPP3T** ($M_w$ = 400 kg mol$^{-1}$) ≤ **HD-PDPP3T*alt*TPT** < **HD-PDPPTPT** < **OD-PDPPTPT** < **DT-PDPPTPT**. b) The solubility of **HD-PDPP3T** is enhanced with decreasing the $M_w$. The red arrows are guides to the eye.

Vertical stratification of BHJ blend films has been widely investigated, but its extent and origin remain debated.[24–26] Differences in surface free energy, solubility, and selective interactions can disrupt the vertical isotropy of the morphology. The extent of vertical stratification is also affected by the processing conditions (e.g., drying rate, solvent or thermal annealing, and presence of top contact). For as-cast P3HT:[60]PCBM blends the surface energy of the substrate was found to control the stratification, resulting in an enrichment of [60]PCBM at the PEDOT:PSS/blend interface in as cast films.[24] In contrast, for as-cast PCDTBT:PCBM blends on PEDOT:PSS an enrichment of PCBM at blend/air surface was found,[27–29] while in as-cast PSBTBT:[60]PCBM blends there is an enrichment of PSBTBT at the free surface.[30] Similar differences also exist for deposition on ZnO. Marks and co-workers reported a [70]PCBM enrichment at ZnO interface,[9] but here we found that at the ZnO surface there is an enrichment in polymer concentration for materials that are more soluble. This could imply, tentatively, that the ZnO layer with its surface ripple nanostructures acts as a preferential site for aggregation of polymers with good solubility, while polymers with less solubility aggregate more homogenously in solution. It is presently not clear how the surface enrichment contributes to the improved performance of inverted devices compared to conventional devices. Further efforts are required to explore the mechanisms and generality of the vertical structure in BHJ blends. Beside the nature of the substrate there are several other factors that influence vertical stratification. For instance, the processing solvent/cosolvent allowed the transition from enriched to depleted fullerene at the interface,[31,32] and pre-/post-treatment had significant impact on vertical phase separation within the whole BHJ blend film.[24,33]

### 2.2. Morphology Control by Cosolvents

It is well established that the cosolvent plays a crucial role in forming the phase separation and BHJ morphology of


© 2018 The Authors. Published by WILEY-VCH Verlag GmbH & Co. KGaA, Weinheim

16146840, 2018, 22, Downloaded from https://onlinelibrary.wiley.com/doi/10.1002/aenm.201800550 by Univ of California Lawrence Berkeley National Lab, Wiley Online Library on [22/02/2024]. See the Terms and Conditions (https://onlinelibrary.wiley.com/terms-and-conditions) on Wiley Online Library for rules of use; OA articles are governed by the applicable Creative Commons License

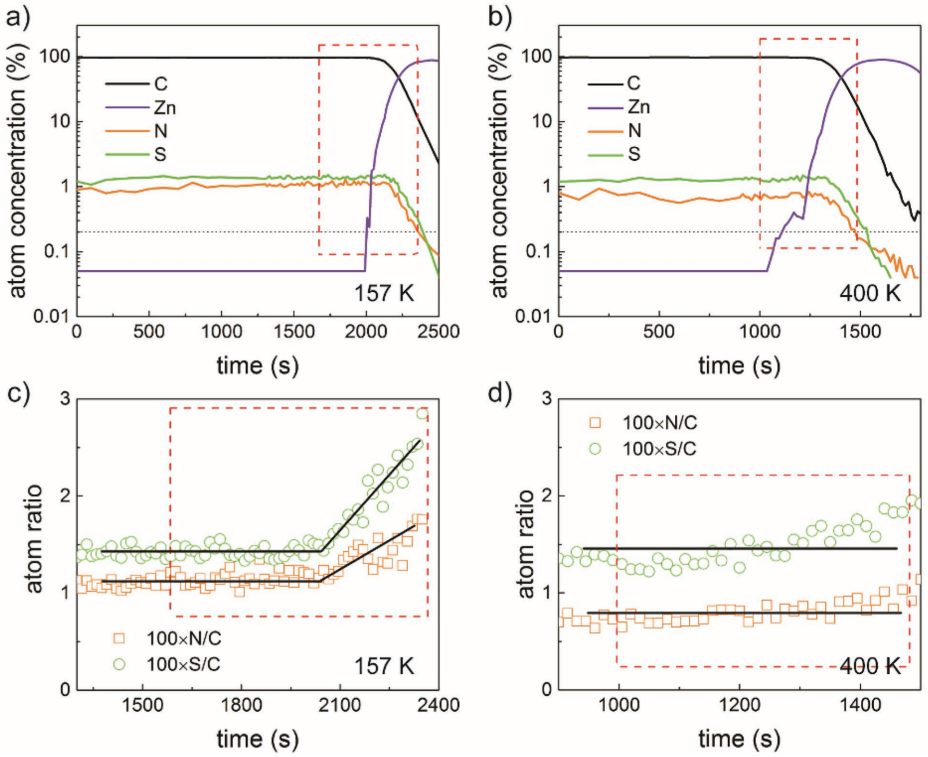


**Figure 7.** a,b) Atom concentrations and c,d) atom ratios from XPS depth profiles of **HD-PDPP3T**:[70]PCBM (1:2 w/w) layers with $M_w$ = 157 and 400 kg mol$^{-1}$ processed on ZnO. Due to the detection limits the data of Zn with the atom concentration below 0.1% are displayed as 0.05%; further the atom ratio is estimated in the range where atom concentration is over 0.2% (red dashed frames).

polymer–fullerene blends, affecting exciton diffusion, charge dissociation, and charge transport.[22] Moreover, it was demonstrated that narrower fibrils promote the photon-to-electron conversion efficiency.[17,34] In Section 2.1, solar cells with the efficiencies of 8.4%, 7.2%, and 7.7% were realized based on **HD-PDPPTPT**, **HD-PDPP3T**, and **HD-PDPP3T*alt*TPT**, respectively, in an inverted polarity device (**Table 2**). Further reducing the fibril width by optimizing the cosolvent is a rational option to realize further improvement of cell performance for these three DPP-based polymers. For **HD-PDPPTPT**, diphenyl ether (DPE) is used to replace *o*-DCB. TEM images reveal that the widths of the fibrils are different and decrease, going from 7.1 nm for 6% *o*-DCB to 5.7 nm for 5% DPE (**Figure 8**a,d). GIWAXS measurements reveal that such slight difference in fibril width has little effect on the molecular orientation but enhances film crystallinity (Figure 8g; Figure S12, Supporting Information). As expected, the OPV device processed with 5% DPE generates more current with $J_{sc,sr}$ = 16.8 mA cm$^{-2}$, which is 1 mA cm$^{-2}$ higher than when using 6% *o*-DCB, resulting in a PCE of 8.6% (**Figure 9**a; Figure S13, Supporting Information). The high performance does not strongly depend on the concentration of the cosolvent as virtually identical results were found using 2% DPE. For **HD-PDPP3T**, the fibril width is significantly reduced from 12.9 to 8.6 nm by using 6% 1,2,4-trichlorobenzene (TCB) as cosolvent, as shown in Figure 8b,e. This length scale (8.6 nm) matches with the exciton diffusion length (5–10 nm),[35] leading to the improved device performance. In the 1D GIWAXS line-cut profile the **HD-PDPP3T**:[70]PCBM layer processed using TCB as cosolvent shows a sharp shoulder peak at $q$ = 1.72 Å$^{-1}$ with a coherence length of 2.2 nm (Figure 8h), while **HD-PDPP3T** with 6% *o*-DCB cosolvent displays a broader peak at $q$ = 1.75 Å$^{-1}$ with $L_{CH}$ = 1.3 nm. The increased $L_{CH}$ implies a more ordered crystallization which can be beneficial for charge separation, resulting in an enhanced $J_{sc,sr}$ from 15.5 to 17.0 mA cm$^{-2}$.[36,37] The resultant PCE of 7.6% is achieved with $EQE_{max}$ = 0.55 (Figure 9a). With 10% *o*-DCB, the fibril width of **HD-PDPP3T*alt*TPT**:[70]PCBM is already comparable to the exciton diffusion length, and the use of 6% TCB is not capable of further optimizing the morphology. Therefore, identical device performance is obtained. Interestingly, 1-chloronaphthalene (CN) with a higher boiling point than TCB allowed to further narrow the fibrils of **HD-PDPP3T*alt*TPT** to 4.3 nm (Figure 8c,f), so that the performance of corresponding solar cell was improved with PCE = 8.4%, $V_{oc}$ = 0.74 V, FF = 0.68, and $J_{sc}$ = 16.6 mA cm$^{-2}$ (Figure 9a; Figure S13, Supporting Information). Similarly $\pi$–$\pi$ stacking interactions are enhanced using 6% CN with smaller fibril width (Figure 8i). Additionally, grazing incident small angle X-ray scattering (GISAXS) was performed to characterize the mesoscale structures (Figure S15, Supporting Information). In all films a weak diffuse shoulder can be observed in the small angle range at $q$ ≈0.01 Å$^{-1}$, similar to the signals found by Russell and co-workers for a related DPP polymer fullerene blend.[38]

The PCE for all five DPP-based polymers with inverted polarity are plotted as a function of fibril width in Figure 9b. It is clear that the cell performance is noticeably enhanced with decreasing the fibril width, and an almost linear correlation is


© 2018 The Authors. Published by WILEY-VCH Verlag GmbH & Co. KGaA, Weinheim

16146840, 2018, 22, Downloaded from https://onlinelibrary.wiley.com/doi/10.1002/aenm.201800550 by Univ of California Lawrence Berkeley National Lab, Wiley Online Library on [22/02/2024]. See the Terms and Conditions (https://onlinelibrary.wiley.com/terms-and-conditions) on Wiley Online Library for rules of use; OA articles are governed by the applicable Creative Commons License

**Table 2.** Solar-cell characteristics.

| Polymer[a)] | $M_w$ kg mol$^{-1}$ | PDI[b)] | Polarity | Cosolvent[d)] | $V_{oc}$ [V] | FF | $J_{sc,sr}$[e)] [mA cm$^{-2}$] | $EQE_{max}$[f)] | $PCE_{max}$ [%] | $PCE_{avg}$[g)] [%] |
|---|---|---|---|---|---|---|---|---|---|---|
| **HD-PDPPTPT** | 143 | 2.0 | conv. | 6% *o*-DCB | 0.80 ± 0.01 | 0.66 ± 0.01 | 13.8 ± 0.2 | 0.58 | 7.4 | 7.3 ± 0.1 |
| | | | inv. | 6% *o*-DCB | 0.80 ± 0.00 | 0.66 ± 0.01 | 15.6 ± 0.3 | 0.66 | 8.4 | 8.3 ± 0.1 |
| | | | inv. | 2% DPE | 0.79 ± 0.00 | 0.62 ± 0.02 | 16.8 ± 0.2 | 0.71 | 8.5 | 8.2 ± 0.2 |
| | | | inv. | 5% DPE | 0.79 ± 0.00 | 0.64 ± 0.02 | 16.7 ± 0.2 | 0.70 | 8.6 | 8.4 ± 0.2 |
| | | | inv+foil[c)] | 5% DPE | 0.80 | 0.64 | 18.7 | 0.71 | 9.6 | – |
| **OD-PDPPTPT** | 442 | 3.2 | conv. | 2.5% DIO | 0.81 ± 0.00 | 0.66 ± 0.01 | 9.6 ± 0.1 | 0.39 | 5.2 | 5.1 ± 0.1 |
| | | | inv. | 2.5% DIO | 0.79 ± 0.00 | 0.71 ± 0.00 | 10.8 ± 0.1 | 0.46 | 6.1 | 6.0 ± 0.0 |
| **DT-PDPPTPT** | 216 | 2.4 | conv. | 5% DIO | 0.79 ± 0.00 | 0.66 ± 0.01 | 8.3 ± 0.1 | 0.31 | 4.4 | 4.4 ± 0.1 |
| | | | inv. | 5% DIO | 0.79 ± 0.01 | 0.70 ± 0.00 | 8.7 ± 0.3 | 0.36 | 4.9 | 4.8 ± 0.1 |
| **HD-PDPP3T** | 79 | 1.9 | conv. | 7.5% *o*-DCB | 0.64 ± 0.00 | 0.65 ± 0.01 | 12.2 ± 0.5 | 0.34 | 5.2 | 5.1 ± 0.1 |
| | | | inv. | 7.5% *o*-DCB | 0.65 ± 0.00 | 0.69 ± 0.01 | 13.5 ± 0.2 | 0.39 | 6.1 | 6.0 ± 0.1 |
| | 157 | 2.1 | conv. | 7.5% *o*-DCB | 0.65 ± 0.01 | 0.64 ± 0.01 | 12.3 ± 0.2 | 0.33 | 5.1 | 5.1 ± 0.0 |
| | | | inv. | 7.5% *o*-DCB | 0.65 ± 0.00 | 0.66 ± 0.01 | 15.0 ± 0.2 | 0.47 | 6.5 | 6.5 ± 0.1 |
| | 255 | 3.7 | conv. | 7.5% *o*-DCB | 0.65 ± 0.00 | 0.66 ± 0.00 | 13.5 ± 0.1 | 0.39 | 5.9 | 5.8 ± 0.1 |
| | | | inv. | 7.5% *o*-DCB | 0.67 ± 0.00 | 0.68 ± 0.00 | 14.8 ± 0.3 | 0.47 | 6.8 | 6.6 ± 0.1 |
| | 400 | 2.7 | conv. | 7.5% *o*-DCB | 0.66 ± 0.00 | 0.68 ± 0.01 | 15.3 ± 0.3 | 0.49 | 7.1 | 6.9 ± 0.1 |
| | | | inv. | 7.5% *o*-DCB | 0.67 ± 0.00 | 0.69 ± 0.01 | 15.3 ± 0.2 | 0.47 | 7.2 | 7.1 ± 0.1 |
| | | | inv. | 6% TCB | 0.67 ± 0.00 | 0.68 ± 0.02 | 16.5 ± 0.5 | 0.55 | 7.6 | 7.4 ± 0.1 |
| | | | inv.+foil[c)] | 6% TCB | 0.67 | 0.66 | 18.8 | 0.57 | 8.3 | – |
| **HD-PDPP3T*alt*TPT** | 154 | 3.7 | conv. | 10% *o*-DCB | 0.73 ± 0.01 | 0.66 ± 0.01 | 16.2 ± 0.4 | 0.59 | 8.0 | 7.8 ± 0.2 |
| | | | inv. | 10% *o*-DCB | 0.74 | 0.64 | 16.3 | 0.61 | 7.7 | – |
| | | | inv. | 6% TCB | 0.75 | 0.62 | 16.7 | 0.63 | 7.8 | – |
| | | | inv. | 6% CN | 0.75 ± 0.00 | 0.66 ± 0.02 | 16.6 ± 0.3 | 0.63 | 8.4 | 8.2 ± 0.1 |

[a)]The weight ratio of polymer to [70]PCBM is 1:2 in all cases; [b)]The weight average molecular weight ($M_w$) and polydispersity index (PDI) of DPP polymers; [c)]A retroreflective foil is applied on the cell; [d)]The host solvent is chloroform in all cases; [e)]$J_{sc,sr}$ is obtained by integrating the EQE spectrum with AM 1.5 G spectrum; [f)]$EQE_{max}$ in the region >700 nm; [g)]The average value is obtained from four nominally identical devices.

observed. When the fibril width is below 10 nm, the efficiency ($\eta$) exceeds 7.5%. In particular, the value of $\eta$ = 8.4–8.6% is achievable with fibril width of 4–6 nm, which can be realized by cosolvent optimization (open symbols in Figure 9b). Typical exciton diffusion lengths for conjugated polymers are 5–10 nm, and therefore wider fibrils may detrimentally influence the percentage of excitons reaching the polymer/fullerene interface where charge generation happens. This assumption is further proven by the relation between fibril width and the maximum value of EQE for wavelength region over 700 nm, where the polymer absorption dominates (Figure S14a, Supporting Information). Fibrils with width lower than 8 nm result in the EQE over 0.60, but fibrils over 10 nm lead to the EQE below 0.50. In addition, our results for conventional devices reveal a good correlation with our previous study (Figure S14b, Supporting Information).[34] More importantly, it is worth noting that this EQE dependence on fibril width is not affected by device polarity.

### 2.3. Enhancement of Light Absorption by Retroreflective Foil

For most DPP-based polymers, the optimum thickness of polymer:[70]PCBM blend films ranges from 90 to 110 nm depending on the device configurations. This is insufficient to quantitatively absorb the light over the whole absorption spectrum. In other words, a non-negligible amount of light is reflected out of the solar cell. Thicker films are able to absorb more light, but in general the fill factor is significantly reduced, contributing to a low PCE. The light capture can be enhanced by changing the trajectory of the light in the solar cell with the application of an additional retroreflective foil.[39–44] As described in Sections 2.1 and 2.2, **HD-PDPPTPT**:[70]PCBM blend films exhibit very good photovoltaic performance (PCE = 8.6%, $V_{oc}$ = 0.79 V, FF = 0.64, $J_{sc,sr}$ = 16.8 mA cm$^{-2}$) in an inverted device configuration using 5% DPE as cosolvent, which is among the best solar cells based on DPP polymers. The application of a retroreflective foil on top of the device allows to effectively absorb more light into active layer,[39] so that a 13.8% improvement in photocurrent is obtained without affecting $V_{oc}$ and FF, resulting in concomitant increase of PCE to 9.6% (**Figure 10**a). The enhanced $J_{sc}$ is confirmed by EQE measurement, indicating an improved quantum efficiency over the whole spectral range, as shown in Figure 10c. The increase in EQE mainly occurs at wavelengths where the absorption of blend film is weaker, such as 400–440 and 550–610 nm. In these regions, more of the incident light is reflected toward to the retroreflective foil.[37]


© 2018 The Authors. Published by WILEY-VCH Verlag GmbH & Co. KGaA, Weinheim

16146840, 2018, 22, Downloaded from https://onlinelibrary.wiley.com/doi/10.1002/aenm.201800550 by Univ of California Lawrence Berkeley National Lab, Wiley Online Library on [22/02/2024]. See the Terms and Conditions (https://onlinelibrary.wiley.com/terms-and-conditions) on Wiley Online Library for rules of use; OA articles are governed by the applicable Creative Commons License

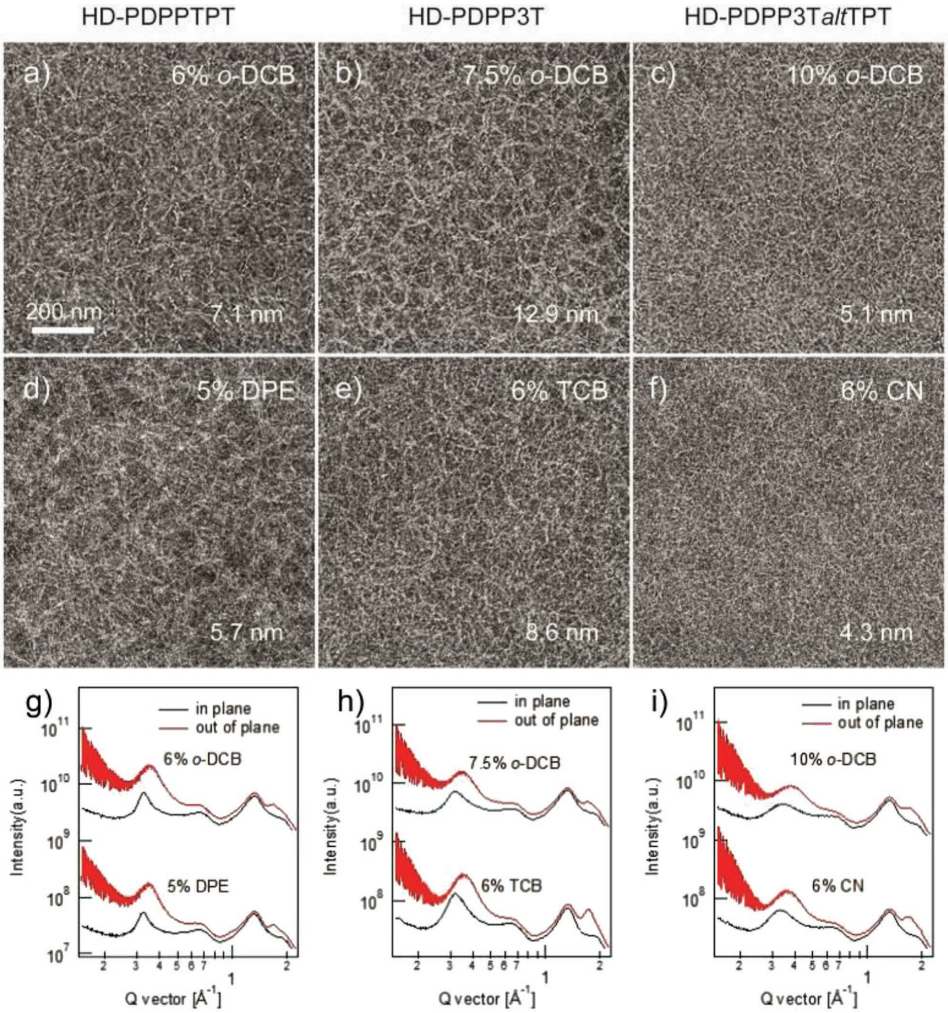


**Figure 8.** TEM images of the photoactive layers with various cosolvents: a,d) **HD-PDPPTPT**:[70]PCBM, b,e) **HD-PDPP3T**:[70]PCBM, and c,f) **HD-PDPP3T*alt*TPT**:[70]PCBM. All images share the same scale bar. Inverted structures are utilized. g–i) The corresponding GIWAXS in-plane and out-of-plane profiles.

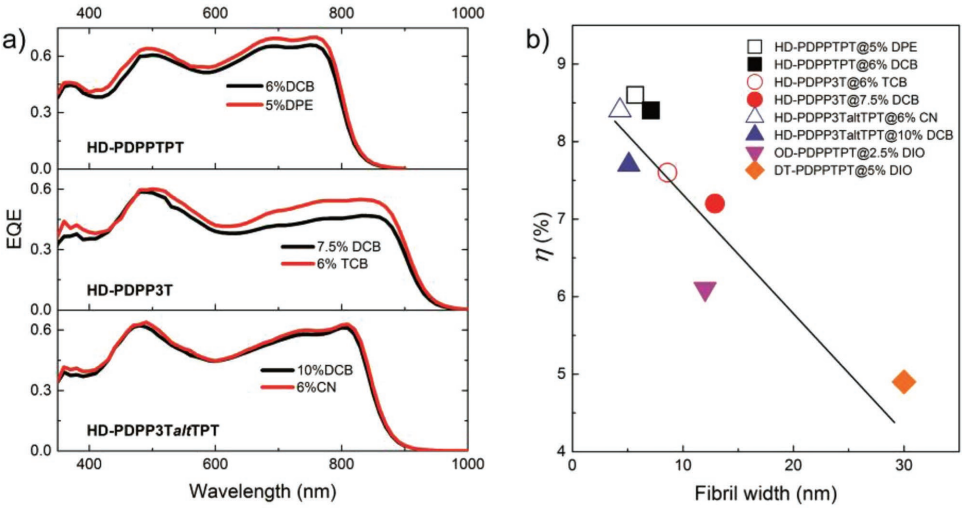


**Figure 9.** a) EQE spectra of **HD-PDPPTPT**:[70]PCBM, **HD-PDPP3T**:[70]PCBM, and **HD-PDPP3T*alt*TPT**:[70]PCBM with various cosolvents. Inverted structures are utilized. b) Dependence of PCE ($\eta$) on the fibril width.


© 2018 The Authors. Published by WILEY-VCH Verlag GmbH & Co. KGaA, Weinheim

16146840, 2018, 22, Downloaded from https://onlinelibrary.wiley.com/doi/10.1002/aenm.201800550 by Univ of California Lawrence Berkeley National Lab, Wiley Online Library on [22/02/2024]. See the Terms and Conditions (https://onlinelibrary.wiley.com/terms-and-conditions) on Wiley Online Library for rules of use; OA articles are governed by the applicable Creative Commons License

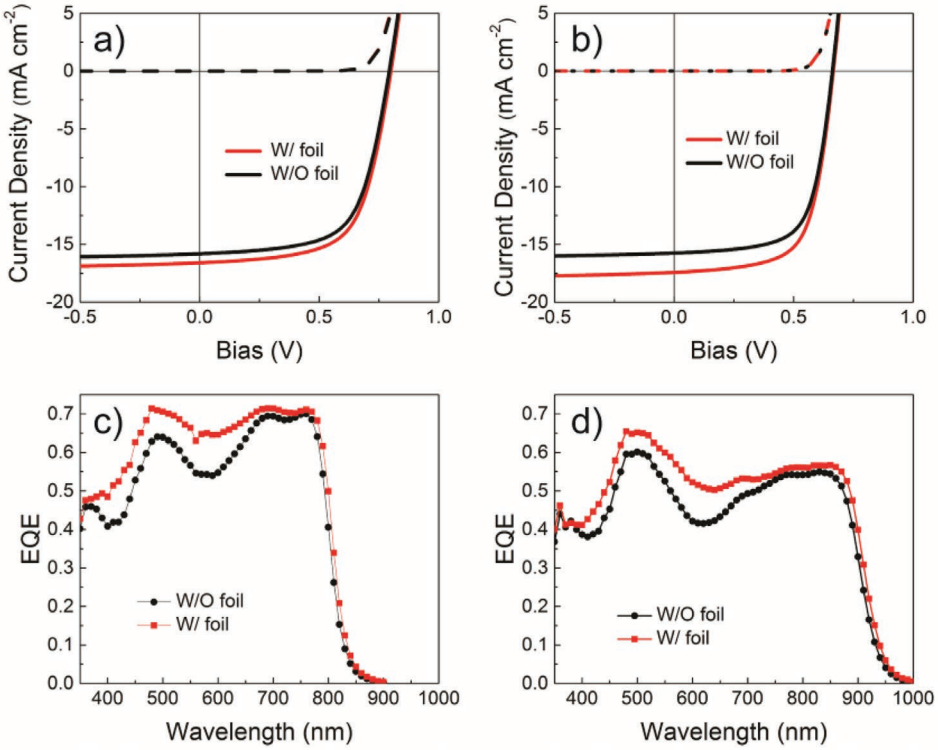


**Figure 10.** *J–V* characteristics and spectrally resolved EQEs of a,c) **HD-PDPPTPT**:[70]PCBM and b,d) **HD-PDPP3T**:[70]PCBM without (W/O) and with (W/) retroreflective foils.

Among the polymers investigated in this study, **HD-PDPP3T** differs most in optical properties from **HD-PDPPTPT**, but also for **HD-PDPP3T** ($M_w$ = 400 kg mol$^{-1}$) the retroreflective foil is capable of improving OPV performance. The light reflected by the foil back into the photoactive layer generates 1.8 mA cm$^{-2}$ of additional current density, and the PCE is significantly increased from 7.6% to 8.3% (Figure 10b,d). Additionally, applying a retroreflective foil allowed capturing more light, significantly enhancing the photocurrent. Combined the effects resulted in a solar cell with PCE of 9.6%, among the best for DPP polymers. Although the results are based on DPP polymers, we consider that the optimization procedures developed here, represent a general framework that is practical to optimize the device performance for all types of organic photovoltaics.

## 3. Conclusion

In conclusion, we demonstrated the optimization of device performance of polymer:fullerene solar cells by manipulating the device polarity, morphology, and light absorption for series of DPP-based polymers. We determined that the polymer solubility, which is controlled by chemical structure and molecular weight, critically affects the optimal device configuration. In the case of polymers with good solubility, an enhancement in photovoltaic performance by 10–25% is obtained by applying an inverted polarity configuration. On the contrary, for less soluble polymers the performance is independent of device polarity. It was found that for more soluble materials the polymer:fullerene ratio in the inverted configuration is slightly increased close to the ZnO interface, while for the less soluble polymers this difference does not occur. Further improvement of device performance was realized by optimizing the cosolvent and employing a retroreflective foil. A careful choice of cosolvent is efficient to reduce the fibril width. The PCE and maximum EQE scale inversely with the fibril width, in good agreement with our previous report.[17] In particular, the PCE of 8.4–8.6% is achievable for fibril widths of 4–6 nm.

## 4. Experimental Section

*Materials*: All **PDPPTPT** polymers were prepared by Suzuki polymerization, in which a catalyst system was used based on $Pd_2(dba)_3$ as palladium source and $PPh_3$ as ligand. Both **HD-PDPP3T** and **HD-PDPP3T*alt*TPT** were synthesized by Stille polymerization. The details of polymer synthesis can be found in literature.[17,45] The molecular weight of **HD-PDPP3T** was varied by controlling the monomer ratio (See the Supporting Information). The molecular weight of all polymers was determined by gel permeation chromatography (GPC) using *o*-DCB as eluent at 140 °C and a low polymer concentration of 0.06 mg mL$^{-1}$ to reduce aggregation.

*Device Fabrication*: Prepatterned ITO substrates (15 Ω per square, Naranjo Substrates) were used for all photovoltaic devices. For devices with the conventional configuration (ITO/PEDOT:PSS/polymer:[70]PCBM/LiF/Al), PEDOT:PSS (Clevios P, VP Al 4083) was spin-coated and annealed at 140 °C for 10 min to form a thin film with final thickness of 40 nm. For inverted devices (ITO/ZnO/polymer:[70]PCBM/$MoO_x$/Ag), a ZnO layer was fabricated by the sol–gel method, where zinc acetate (109.7 mg) was dissolved into 2-methoxyethanol (1 mL) with ethanol amine (30.2 µL). Spin-coated films were annealed at 140 °C for 10 min. The final thickness was 40 nm. All photoactive layers were deposited by spin-coating from a chloroform solution with different cosolvents. LiF (1 nm) and Al (100 nm), or $MoO_x$ (10 nm) and Ag (100 nm) were deposited as back contacts by vacuum evaporation at ≈2 × 10$^{-7}$ mbar.


© 2018 The Authors. Published by WILEY-VCH Verlag GmbH & Co. KGaA, Weinheim

16146840, 2018, 22, Downloaded from https://onlinelibrary.wiley.com/doi/10.1002/aenm.201800550 by Univ of California Lawrence Berkeley National Lab, Wiley Online Library on [22/02/2024]. See the Terms and Conditions (https://onlinelibrary.wiley.com/terms-and-conditions) on Wiley Online Library for rules of use; OA articles are governed by the applicable Creative Commons License

The active area of the cells was 0.09 or 0.16 $cm^2$, and no dependence of photovoltaic performance on the active area was found.

*Characterizations*: The white light (≈100 mW $cm^{-2}$) from a tungsten–halogen lamp filtered by a Schott GG385 UV filter and a Hoya LB120 daylight filter was used for illumination, and *J–V* characteristics were measured using a Keithley 2400 source meter. Short-circuit currents under AM1.5G conditions were estimated from the EQE and integration with the solar spectrum. The EQE was recorded by a lock-in amplifier (Stanford Research Systems SR 830) under simulated 1 sun operation conditions with bias light from a 532 nm solid state laser (Edmund Optics). As probe light, the light from a 50 W tungsten halogen lamp (Osram64610) was modulated with a mechanical chopper before passing the monochromator (Oriel, Cornerstone 130) for wavelength selection. A calibrated Si cell was used as reference. Polymer solar cells were kept behind a quartz window in a nitrogen filled container. TEM measurement (Tecnai $G^2$ Sphera, FEI) was carried out at 200 kV. XPS depth profiles were measured on a Thermo Scientific K-Alpha with a 180° double focusing hemispherical analyzer and a 128-channel detector. The layers were removed in steps by argon ion etching at low current and 1000 eV ion energy ($Ta_2O_5$ = 0.12 nm $s^{-1}$).

*GIWAXS*: GIWAXS measurements were performed at beamline 7.3.3[46] at the Advanced Light Source. The $Si/SiO_2$ wafers coated with 40 nm PEDOT:PSS were used as substrates. Samples were prepared on $Si/SiO_2$/PEDOT:PSS substrates using identical blend solutions as those used in devices. The 10 keV X-ray beam was incident at a grazing angle of 0.12°–0.16°, selected to maximize the scattering intensity from the samples. The scattered X-rays were detected using a Dectris Pilatus 2M photon counting detector. The coherence length in direction perpendicular to the (010) crystallographic plane was calculated using the Scherrer equation[47–49]

$$L_{CH} = \frac{2\pi K}{\Delta q} \tag{1}$$

where $\Delta q$ is the full-width at half-maximum of the peak and $K$ is a shape factor with the empirical value of 0.9. The Bragg peaks are fitted to the positions and widths with a linear background. It must be emphasized that the width of the Bragg peak is strongly affected by both paracrystallinity[50] and instrumental effects. Therefore, care must be taken when using Scherrer equation, and such analysis only provides qualitative comparison between samples with rough estimations of coherence length, also because we have used slightly different incident angles.

*GISAXS*: GISAXS experiments were carried out on a GANESHA 300XL+ system from JJ X-ray in the X-ray lab at DSM Materials Sciences Center (DMSC). The instrument is equipped with a Pilatus 300K detector, with pixel size of 172 µm × 172 µm. The X-ray source is a Genix 3D Microfocus Sealed Tube X-Ray Cu-source with integrated Monochromator (multilayer optic "3D version" optimized for SAXS) (30 W). The wavelength used was $\lambda$ = 1.5408 Å. The detector moved in a vacuum chamber with sample-to-detector distance varied between 0.115 and 1.47 m depending on the configuration used, as calibrated using silver behenate ($d_{001}$ = 58.38 Å). The minimized background scattering plus high-performance detector, allowed for a detectable $q$-range varying from $3 \times 10^{-3}$ to 3 $Å^{-1}$ (0.2 to 210 nm). The sample was placed vertically on the goniometer and tilted to a glancing angle of 0.2° with respect to the incoming beam. A large beam was used to increase the signal to noise ratio. The primary slits had a size of 0.7 × 0.7 $mm^2$, and the guard slits had a size of 0.1 × 0.9 $mm^2$. The accumulation time was 6 h for each measurement.

## Supporting Information

Supporting Information is available from the Wiley Online Library or from the author.

## Acknowledgements

This project has received funding from the European Union's Horizon 2020 research and innovation programme under the Marie Skłodowska-Curie grant agreement No. 747422. W.M. thanks for the support from Ministry of science and technology (No. 2016YFA0200700), NSFC (21504066, 21534003), and Open Research Fund of State Key Laboratory of Polymer Physics and Chemistry, Changchun Institute of Applied Chemistry, Chinese Academy of Sciences. X-ray data were acquired at beamlines 7.3.3 at the Advanced Light Source, which is supported by the Director, Office of Science, Office of Basic Energy Sciences, of the U.S. Department of Energy under Contract No. DE-AC02-05CH11231. The authors thank Chenhui Zhu at beamline 7.3.3, for assistance with data acquisition. The research also received funding from the European Research Council under the European Union's Seventh Framework Programme (FP/2007-2013)/ERC Grant Agreement No. 339031 and from the Ministry of Education, Culture and Science (Gravity program 024.001.035).

## Conflict of Interest

The authors declare no conflict of interest.

## Keywords

device polarity, light absorption, morphology control, polymer solar cells

Received: February 16, 2018
Revised: March 15, 2018
Published online: May 16, 2018

[1] G. Li, R. Zhu, Y. Yang, *Nat. Photonics* **2012**, *6*, 153.
[2] B. C. Thompson, J. M. J. Fréchet, *Angew. Chem., Int. Ed.* **2008**, *47*, 58.
[3] S. Holliday, Y. Li, C. K. Luscombe, *Prog. Polym. Sci.* **2017**, *70*, 34.
[4] W. Li, K. H. Hendriks, M. M. Wienk, R. A. J. Janssen, *Acc. Chem. Res.* **2016**, *49*, 78.
[5] W. Li, K. H. Hendriks, A. Furlan, A. Zhang, M. M. Wienk, R. A. J. Janssen, *Chem. Commun.* **2015**, *51*, 4290.
[6] A. P. Zoombelt, S. G. J. Mathijssen, M. G. R. Turbiez, M. M. Wienk, R. A. J. Janssen, *J. Mater. Chem.* **2010**, *20*, 2240.
[7] K. H. Hendriks, W. Li, M. M. Wienk, R. A. J. Janssen, *J. Am. Chem. Soc.* **2014**, *136*, 12130.
[8] W. Li, K. H. Hendriks, A. Furlan, M. M. Wienk, R. A. J. Janssen, *J. Am. Chem. Soc.* **2015**, *137*, 2231.
[9] X. Guo, N. Zhou, S. J. Lou, J. Smith, D. B. Tice, J. W. Hennek, R. P. Ortiz, J. T. L. Navarrete, S. Li, J. Strzalka, L. X. Chen, R. P. H. Chang, A. Facchetti, T. J. Marks, *Nat. Photonics* **2013**, *7*, 825.
[10] Z. He, C. Zhong, S. Su, M. Xu, H. Wu, Y. Cao, *Nat. Photonics* **2012**, *6*, 591.
[11] R. S. Ashraf, I. Meager, M. Nikolka, M. Kirkus, M. Planells, B. C. Schroeder, S. Holliday, M. Hurhangee, C. B. Nielsen, H. Sirringhaus, I. McCulloch, *J. Am. Chem. Soc.* **2015**, *137*, 1314.
[12] T. Ma, K. Jiang, S. Chen, H. Hu, H. Lin, Z. Li, J. Zhao, Y. Liu, Y.-M. Chang, C.-C. Hsiao, H. Yan, *Adv. Energy Mater.* **2015**, *5*, 1501282.
[13] M. S. Vezie, S. Few, I. Meager, G. Pieridou, B. Dorling, R. S. Ashraf, A. R. Goni, H. Bronstein, I. McCulloch, S. C. Hayes, M. Campoy-Quiles, J. Nelson, *Nat. Mater.* **2016**, *15*, 746.
[14] X.-P. Xu, G.-J. Zhang, Y.-z. Zhao, J. Liu, Y. Li, Q. Peng, *Chin. J. Polym. Sci.* **2017**, *35*, 249.
[15] H. Choi, S.-J. Ko, T. Kim, P.-O. Morin, B. Walker, B. H. Lee, M. Leclerc, J. Y. Kim, A. J. Heeger, *Adv. Mater.* **2015**, *27*, 3318.
[16] Y. Liu, G. Li, Z. Zhang, L. Wu, J. Chen, X. Xu, X. Chen, W. Ma, Z. Bo, *J. Mater. Chem. A* **2016**, *4*, 13265.
[17] W. Li, K. H. Hendriks, A. Furlan, W. S. C. Roelofs, S. C. J. Meskers, M. M. Wienk, R. A. J. Janssen, *Adv. Mater.* **2014**, *26*, 1565.


© 2018 The Authors. Published by WILEY-VCH Verlag GmbH & Co. KGaA, Weinheim

16146840, 2018, 22, Downloaded from https://onlinelibrary.wiley.com/doi/10.1002/aenm.201800550 by Univ of California Lawrence Berkeley National Lab, Wiley Online Library on [22/02/2024]. See the Terms and Conditions (https://onlinelibrary.wiley.com/terms-and-conditions) on Wiley Online Library for rules of use; OA articles are governed by the applicable Creative Commons License

[18] J. C. Bijleveld, V. S. Gevaerts, D. Di Nuzzo, M. Turbiez, S. G. J. Mathijssen, D. M. de Leeuw, M. M. Wienk, R. A. J. Janssen, *Adv. Mater.* **2010**, *22*, E242.
[19] Z. Liang, Q. Zhang, L. Jiang, G. Cao, *Energy Environ. Sci.* **2015**, *8*, 3442.
[20] S. Nho, G. Baek, S. Park, B. R. Lee, M. J. Cha, D. C. Lim, J. H. Seo, S.-H. Oh, M. H. Song, S. Cho, *Energy Environ. Sci.* **2016**, *9*, 240.
[21] J. Gilot, I. Barbu, M. M. Wienk, R. A. J. Janssen, *Appl. Phys. Lett.* **2007**, *91*, 113520.
[22] J. J. van Franeker, G. H. L. Heintges, C. Schaefer, G. Portale, W. Li, M. M. Wienk, P. van der Schoot, R. A. J. Janssen, *J. Am. Chem. Soc.* **2015**, *137*, 11783.
[23] J. C. Bijleveld, A. P. Zoombelt, S. G. J. Mathijssen, M. M. Wienk, M. Turbiez, D. M. de Leeuw, R. A. J. Janssen, *J. Am. Chem. Soc.* **2009**, *131*, 16616.
[24] M. Campoy-Quiles, T. Ferenczi, T. Agostinelli, P. G. Etchegoin, Y. Kim, T. D. Anthopoulos, P. N. Stavrinou, D. D. C. Bradley, J. Nelson, *Nat. Mater.* **2008**, *7*, 158.
[25] Z. Li, K. Ho Chiu, R. Shahid Ashraf, S. Fearn, R. Dattani, H. Cheng Wong, C.-H. Tan, J. Wu, J. T. Cabral, J. R. Durrant, *Sci. Rep.* **2015**, *5*, 15149.
[26] Y. Yan, X. Liu, T. Wang, *Adv. Mater.* **2017**, *29*, 1601674.
[27] P. A. Staniec, A. J. Parnell, A. D. F. Dunbar, H. Yi, A. J. Pearson, T. Wang, P. E. Hopkinson, C. Kinane, R. M. Dalgliesh, A. M. Donald, A. J. Ryan, A. Iraqi, R. A. L. Jones, D. G. Lidzey, *Adv. Energy Mater.* **2011**, *1*, 499.
[28] T. Wang, N. W. Scarratt, H. Yi, A. D. F. Dunbar, A. J. Pearson, D. C. Watters, T. S. Glen, A. C. Brook, J. Kingsley, A. R. Buckley, M. W. A. Skoda, A. M. Donald, R. A. L. Jones, A. Iraqi, D. G. Lidzey, *Adv. Energy Mater.* **2013**, *3*, 505.
[29] C.-H. Tan, H. C. Wong, Z. Li, D. G. Bucknall, J. R. Durrant, J. T. Cabral, *J. Mater. Chem. C* **2015**, *3*, 9551.
[30] H. Lu, B. Akgun, T. P. Russell, *Adv. Energy Mater.* **2011**, *1*, 870.
[31] M. Kim, J.-H. Kim, H. H. Choi, J. H. Park, S. B. Jo, M. Sim, J. S. Kim, H. Jinnai, Y. D. Park, K. Cho, *Adv. Energy Mater.* **2014**, *4*, 1300612.
[32] N. Herath, S. Das, J. K. Keum, J. Zhu, R. Kumar, I. N. Ivanov, B. G. Sumpter, J. F. Browning, K. Xiao, G. Gu, P. Joshi, S. Smith, V. Lauter, *Sci. Rep.* **2015**, *5*, 13407.
[33] D. Chen, A. Nakahara, D. Wei, D. Nordlund, T. P. Russell, *Nano Lett.* **2011**, *11*, 561.
[34] W. Li, K. H. Hendriks, A. Furlan, W. S. C. Roelofs, M. M. Wienk, R. A. J. Janssen, *J. Am. Chem. Soc.* **2013**, *135*, 18942.
[35] P. E. Shaw, A. Ruseckas, I. D. W. Samuel, *Adv. Mater.* **2008**, *20*, 3516.
[36] Y. Wu, Z. Y. Wang, X. Y. Meng, W. Ma, *Prog. Chem.* **2017**, *29*, 93.
[37] L. Zhang, W. Ma, *Chin. J. Polym. Sci.* **2017**, *35*, 184.
[38] F. Liu, Y. Gu, C. Wang, W. Zhao, D. Chen, A. L. Briseno, T. P. Russell, *Adv. Mater.* **2012**, *24*, 3947.
[39] S. Esiner, T. Bus, M. M. Wienk, K. Hermans, R. A. J. Janssen, *Adv. Energy Mater.* **2013**, *3*, 1013.
[40] J. D. Myers, W. Cao, V. Cassidy, S.-H. Eom, R. Zhou, L. Yang, W. You, J. Xue, *Energy Environ. Sci.* **2012**, *5*, 6900.
[41] A. Scheydecker, A. Goetzberger, V. Wittwer, *Sol. Energy* **1994**, *53*, 171.
[42] J. Grandidier, R. A. Weitekamp, M. G. Deceglie, D. M. Callahan, C. Battaglia, C. R. Bukowsky, C. Ballif, R. H. Grubbs, H. A. Atwater, *Phys. Status Solidi A* **2013**, *210*, 255.
[43] J. Grandidier, D. M. Callahan, J. N. Munday, H. A. Atwater, *Adv. Mater.* **2011**, *23*, 1272.
[44] S. D. Zilio, K. Tvingstedt, O. Inganäs, M. Tormen, *Microelectron. Eng.* **2009**, *86*, 1150.
[45] K. H. Hendriks, G. H. L. Heintges, V. S. Gevaerts, M. M. Wienk, R. A. J. Janssen, *Angew. Chem., Int. Ed.* **2013**, *52*, 8341.
[46] H. Alexander, B. Wim, G. James, S. Eric, G. Eliot, K. Rick, M. Alastair, C. Matthew, R. Bruce, P. Howard, *J. Phys.: Conf. Ser.* **2010**, *247*, 012007.
[47] A. L. Patterson, *Phys. Rev.* **1939**, *56*, 978.
[48] L. Ye, W. Zhao, S. Li, S. Mukherjee, J. H. Carpenter, O. Awartani, X. Jiao, J. Hou, H. Ade, *Adv. Energy Mater.* **2017**, *7*, 1602000.
[49] G. M. Su, T. V. Pho, N. D. Eisenmenger, C. Wang, F. Wudl, E. J. Kramer, M. L. Chabinyc, *J. Mater. Chem. A.* **2014**, *2*, 1781.
[50] J. Rivnay, S. C. B. Mannsfeld, C. E. Miller, A. Salleo, M. F. Toney, *Chem. Rev.* **2012**, *112*, 5488.


© 2018 The Authors. Published by WILEY-VCH Verlag GmbH & Co. KGaA, Weinheim

16146840, 2018, 22, Downloaded from https://onlinelibrary.wiley.com/doi/10.1002/aenm.201800550 by Univ of California Lawrence Berkeley National Lab, Wiley Online Library on [22/02/2024]. See the Terms and Conditions (https://onlinelibrary.wiley.com/terms-and-conditions) on Wiley Online Library for rules of use; OA articles are governed by the applicable Creative Commons License